



Bioactive fish scale incorporated chitosan biocomposite scaffolds for bone tissue engineering

Aylin Kara^a, Sedef Tamburaci^{a,b}, Funda Tihminlioglu^{b,*}, Hasan Havitcioglu^c

^a Biotechnology and Bioengineering Graduate Program, Izmir Institute of Technology, Urla, Izmir, Turkey

^b Department of Chemical Engineering, Izmir Institute of Technology, Urla, Izmir, Turkey

^c Department of Orthopedics and Traumatology, Dokuz Eylul University, Izmir, Turkey

ARTICLE INFO

Article history:

Received 30 August 2018

Received in revised form 1 February 2019

Accepted 11 February 2019

Available online 20 February 2019

Keywords:

Fish scale

CH

Composite scaffold

Bone tissue engineering

ABSTRACT

Recently, biologically active natural macromolecules have come into prominence to be used as potential materials in scaffold design due to their unique characteristics which can mimic the human tissue structure with their physical and chemical similarity. Among them, fish scale (FS) is a biologically active material with its structural similarity to bone tissue due to including type I collagen and hydroxyapatite and also have distinctive collagen arrangement. In the present study, it is aimed to design a novel composite scaffold with FS incorporation into chitosan (CH) matrix for bone tissue regeneration. Therefore, two biological macromolecules, fish scale and chitosan, were combined to produce bio-composite scaffold. First, FS were decellularized with the chemical method and disrupted physically as microparticles (100 μm), followed by dispersal in CH with ultrasonic homogenisation, CH/FS scaffolds were fabricated by lyophilization technique. Scaffolds were characterized physically, chemically, mechanically, and morphologically. SEM and porosity results showed that CH/FS scaffolds have uniform pore structure showing high porosity. Mechanical properties and degradation rate are enhanced with increasing FS content. In vitro cytotoxicity, proliferation and osteogenic activity of the scaffolds were evaluated with SaOS-2 cell line. CH/FS scaffolds did not show any cytotoxicity effect and the cells were gradually proliferated during culture period. Cell viability results showed that, FS microparticles had a proliferative effect on SaOS-2 cells when compared to control group. ALP activity and biomineralization studies indicated that FS microparticle reinforcement increased osteogenic activity during culture period. As a biological macromolecule with unique characteristics, FS was found as cytocompatible and provided promising effects as reinforcement agents for polymeric scaffolds. In conclusion, fabricated CH/FS bio-composites showed potential for bone tissue engineering applications.

© 2019 Elsevier B.V. All rights reserved.

1. Introduction

Bone tissue engineering is a complex process that includes migration of osteoprogenitor cells and their proliferation, differentiation, matrix formation along with remodelling of the bone [1]. Bone tissue engineering focus on several key parameters: (i) a scaffold that can mimic the natural bone extracellular matrix, (ii) osteogenic cells to produce the bone tissue matrix, (iii) biochemical signals that help to direct the cells to the phenotypically desirable type, and (iv) sufficient vascularization for the nutrient supply and clearance needs [2]. Design of the scaffolds for bone tissue engineering requires the biocompatibility, biodegradability, flexibility and porosity, as well as sufficient mechanical strength that provide formation of the new tissue. In addition to these properties, materials should provide both osteoinductive (promoting

the differentiation of progenitor cells) and osteoconductive (support bone growth) also capable of osseous-integration (integrate into surrounding bone) [3].

Extensive studies have reported using different synthetic (PCL, PLA, PGA, PEG, PLGA) and natural materials to produce scaffolds for bone tissue engineering [4]. Many natural polymers showed similar chemical properties to bone tissue such as collagen, proteoglycan, elastin, hyaluronic acid (HA), hydroxyapatite (HAp) although synthetic scaffolds are easy to process and can be created with tailored properties (porosity, degradation rate, mechanical strength) but they are often hydrophobic and lack of cell recognition site [1,5–7]. Synthetic polymers have many advantages in terms of scaffold production. However, natural polymers can support tissue regeneration and new tissue formation due to their chemical content as well as bioactivity. Besides degradation byproduct of natural polymers does not have toxic effect and they can be removed from body [8]. Among natural polymers, CH is mostly preferred for tissue engineering applications with its promising

* Corresponding author.

E-mail address: fundatihminlioglu@iyte.edu.tr (F. Tihminlioglu).

characteristics such as biocompatibility and biodegradability with non-toxic by products. Besides, CH has structural similarity with extracellular matrix components of tissues, antimicrobial activity and ease of processing [9,10]. Generally, synthetic and natural polymers have relatively poor load bearing capacity when used alone, with low elastic moduli. Thus, composite scaffolds are preferred with enhanced mechanical properties, degradation rate and biocompatibility. Besides, bone has a nanocomposite structure including inorganic HAp crystals and organic extracellular matrix components mainly composed of type I collagen. Inorganic reinforcements are also used in polymeric matrices to mimic the structure. The nanocomposite structure of bone has a hierarchical organization that include non-mineralized organic component (type I collagen) and mineralized inorganic component (apatite minerals). This nanocomposite structure formed by flexible collagen fibers and HAp crystals is complementary to the compressive strength and high fracture resistance of bone [2].

Elasmoid scale of the teleost fish are highly ordered three-dimensional structure showing similarity to bone and it is composed of extracellular matrix, mainly type I collagen fibers and HAp [11]. In cross section, FS consist of two layers; external (osseous) layer has randomly arranged collagen fibers and fibrillary internal (basal plate) layer which collagen fibers are organized into lamellae to produce an orthogonal plywood-like arrangement. The collagen fibrils on each layer are oriented approximately 90° [11]. Scleroblasts are located at the base of the scales and produced collagen fibers [12]. The microchannels are organized through the consecutive fibers that involvement of microtubules and microfilaments during the formation of the patterned plate [13]. The distinct organization of fibers is the key factor for improved mechanical properties [11]. Mineralization of the scales occurs with the accumulation of the HAp between collagen fibers. Needle-like HAp crystals distributed through the aligned collagen fibers in the internal layer of the FS [14].

The studies about FS are mostly containing the extraction of collagen [15–18] and HAp [19–21] for producing scaffolds for bone tissue engineering generally [22]. Besides, there are studies on the evaluating biocompatibility of FS. Fang et al. evaluated the structural and the biocompatibility properties of FS from *Carassius auratus* and they claimed that fish scales are cytocompatible for fibroblast like cells and cells proliferate and migrate along the channels of the FS [23]. Moreover, Yamamoto et al. reported that the collagen obtained from FS is biologically safe for skin and bone applications [24]. FS is a biodegradable and inexpensive biological source. In addition, its structural similarity to the bone extracellular matrix, therefore is valuable for tissue engineering applications. However, there is no study concerning the use of FS as a reinforcement in polymeric scaffolds. To the best of our knowledge, this is the first time the FS has been used as a size of microparticle incorporate into CH matrix to fabricate a composite scaffold for bone tissue engineering applications.

The aim of the present study is to develop novel composite scaffolds which are composed of FS and CH, that can be used as an implantable material for bone tissue engineering applications. The effect of FS incorporation on the mechanical, physical, morphological properties of scaffolds was investigated. In addition, in vitro cytotoxicity, cell proliferation, osteogenic activity and biomineralization were investigated using SaOS-2 cell line.

2. Material and methods

Chitosan with medium molecular weight powder was purchased from Sigma-Aldrich and used for preparation of composites. *Sparus aurata* fishes were obtained from a commercial dealer in Izmir. Filter (Partec CellTrics, Fisher Scientific) was used with 100 µm mesh diameters to obtain FS microparticle. Tris hydrochloride (Tris-HCl), ethylenediaminetetraacetic acid (EDTA) and sodium dodecyl sulfate (SDS) were used for decellularization process and supplied from Applichem. WST-1 cell proliferation reagent (BioVision Inc.) and StemTAG ALP Assay kit

(Cell Biolabs Inc.), Enzyline PAL Optimise, ALP Kit (Biomerieux Inc.), Human Osteocalcin (OC/BGP) ELISA Kit (Elabscience) were used for in vitro assays. DAPI (Sigma Aldrich) and Alexa Fluor 488 (Thermo Fisher Scientific) were used for fluorescence staining. Materials were used for histological stainings were Hematoxylin&eosin (Surgipath), Masson Trichrome (GBL, Turkey), Type I collagen antibody (Bioss, bs0578-R, Pro-Collagen I Polyclonal Antibody) and type II collagen antibody (Abcam, ab34712, Rabbit Polyclonal Collagen II Antibody). Alizarin Red S and von Kossa were purchase from Sigma, Aldrich. DMEM (Capricorn Scientific) and all supplements (Lonza) were used for cell culture study.

2.1. Decellularization of *Sparus aurata* scales

Fish scales (FS) were harvested from *Sparus aurata* and cleaned with distilled water several times. FS were decellularized based on a modification of the method described previously [25,26]. Initially FS were incubated in 10 mM Tris-HCl buffer and 0.1% EDTA at 4 °C for 24 h. Then 0.1% SDS in Tris-HCl buffer was used to remove the cellular component of the FS at 4 °C for 3 days. Finally, the scales were rinsed with 70% ethanol for sterilization and stored in sterilized phosphate-buffered saline (PBS, pH 7.4) at 4 °C before further application.

Decellularization process was confirmed by SEM, fluorescence microscopy, and histological staining. DAPI was used for fluorescence microscopy and FS were stained with Hematoxyline & eosin, Masson trichrome, type I and type II collagen for the histological evaluation.

2.2. Preparation of CH/FS composite scaffolds

CH/FS composite scaffolds were fabricated by the freeze-drying method. FS were fragmented physically using a mixer and filtered with 100 µm mesh diameter as microparticles. Before use FS microparticles were dried at 45 °C for 24 h in order to remove moisture and prevent agglomeration. CH solution (1 wt%) was prepared by dissolving CH in 1% v/v acetic acid and FS microparticles were dispersed in distilled water for 24 h, separately. Then, they were mixed for 24 h. Ultrasonication (Misonix Ultrasonic Liquid Processor) was used for homogenous dispersion of FS particles in CH matrix for 30 min at 15 °C and 35 Amplitude. The composite dispersion was placed into 48 well plate and prefreezed at –20 °C for 24 h. Lyophilization process was carried out at –46 °C and 0.018 mbar vacuum. Samples were neutralized with 1 M NaOH solution to neutralize remaining acetic acid residues. Prepared CH/FS composite scaffolds were washed with distilled water to remove remaining NaOH.

2.3. Characterization of CH/FS composite scaffolds

2.3.1. Stereomicroscopy and scanning electron microscopy (SEM) analyses

Structure of CH/FS scaffolds were observed under stereomicroscopy (Olympus, SOIF DA 0737). In addition, CH/FS composite scaffolds were analyzed by SEM in order to observe surface morphology, pore size and distribution of FS microparticles in CH matrix. Samples were coated with a thin gold layer under argon gas by using Emitech K550X before analysis. SEM analysis was performed with Quanta FEG scanning electron microscopy (FEI, Thermo Fisher Scientific). Average pore size was calculated with Image J Software. Pore size distribution of scaffolds was analyzed with Minitab software.

2.3.2. Porosity determination with liquid displacement method

Open porosity % of scaffolds was determined with liquid displacement method. Scaffolds were immersed in ethanol (V_1) using the graduated cylinder and incubated in vacuum oven to remove air bubbles in the porous structure. The total volume of scaffold with ethanol is recorded as V_2 . Then scaffolds were removed from ethanol and volume differences were calculated as skeleton of scaffold ($V_2 -$

V_1). Residual ethanol is measured as V_3 . Calculation of open porosity is defined as:

$$\varepsilon = (V_1 - V_3) / (V_2 - V_3) \quad (1)$$

2.3.3. Mechanical properties of composite scaffolds

Mechanical properties of CH/FS composite scaffolds were evaluated with compression test (TA-XT Plus Texture Analyzer) according to ASTM-D 5024-95a standard. Compression was carried out with 5 mm/min cross head speed up to 75% strain. Compressive stress-strain curves were determined, and compressive elastic modulus and maximum stress were calculated for all scaffolds based on the stress and stress data. Mechanical compression data are described as an average of five test specimens with standard error.

2.3.4. Water absorption capacity

Swelling behavior of CH/FS composite scaffolds was evaluated by immersing the lyophilized scaffolds in PBS. Briefly, dry samples were weighted and noted as W_d samples. Then samples were immersed in $1 \times$ PBS (phosphate buffered saline) at 37°C for 1 h, 24 and 48 h periods. The swollen scaffolds were removed and weighed (W_w) after removal of excess surface water using filter paper. Experiments were performed thrice, and water absorption capacity was measured with three samples for each group. The water absorption capacity of composite scaffolds was calculated using following equation:

$$\text{Water Absorption} = (W_w - W_d) / W_d \times 100 \quad (2)$$

2.3.5. Fourier transform infrared spectroscopy (FTIR)

The chemical composition and alterations on bond structures of CH/FS composite scaffolds after degradation were determined by Fourier transform infrared spectroscopy with ATR instrument (FTIR-ATR, Perkin Elmer) at wavenumber range of $4000\text{--}450\text{ cm}^{-1}$ with resolution of 4 cm^{-1} .

2.3.6. Enzymatic degradation of composite scaffolds

Enzymatic degradation was investigated by SEM analysis and weight loss determination at 7, 14, 21 and 28 days of incubation to observe the morphological and structural changes during degradation process. Stability of CH/FS composite scaffolds was evaluated at 37°C with PBS (pH 7.4) containing $1.5\text{ }\mu\text{g/mL}$ lysozyme in order to mimic human serum. 0.01% sodium azide was used to prevent bacterial contamination. The degradation medium was changed every 48 h to ensure continuous enzymatic activity. Weight loss % of samples was investigated for 7, 14, 21 and 28-day incubation periods. The extent of enzymatic degradation was expressed as percentage of weight loss of the dried scaffolds after lysozyme treatment. Enzymatic degradation was indicated by weight loss % calculated using Eq. (3). as shown below;

$$\text{Weight loss\%} = \frac{\text{Initial weight} - \text{Dry weight}}{W_0} \times 100 \quad (3)$$

2.4. In vitro studies

2.4.1. Cell proliferation

SaOS-2 human osteosarcoma cells were sub-cultured in DMEM supplemented with 10% fetal bovine serum (FBS), 1% L-glutamine and 1% streptomycin/penicillin at 37°C in a humidified 5% CO_2 atmosphere. CH/FS composite scaffolds were sterilized with 70% (v/v) ethanol overnight at room temperature before cells seeding. Scaffolds were washed with 1XPBS thrice to remove ethanol and then, scaffolds were immersed in cell culture medium for 3 h at 37°C to allow the cell attachment. 2×10^6 cell/scaffold were seeded on composite scaffolds (1

$\times 1\text{ cm}$) and incubated at 37°C , 5% CO_2 for 21 days. The culture medium was changed twice a week during incubation period. WST1 cell proliferation assay was used to detect metabolic activity of cells. The absorbance was measured by plate reader (Varioskan Flash, ThermoFisher Scientific) at 440 nm wavelength.

2.4.2. Cell attachment

SaOS-2 cells incubated on CH/FS composite scaffolds for 14 days and analyzed with SEM and fluorescence microscopy. For fluorescence observation, cells on the scaffold surface were fixed with 3.7% paraformaldehyde (v/v) in PBS solution for 20 min at room temperature. Samples were washed with $1 \times$ PBS solution and 0.1% Triton X-100 were used for permeabilization. SaOS-2 cells on the scaffold surfaces were stained with DAPI and Alexa flour 555 for observation of the cell nuclei and cytoskeleton and visualized by fluorescence microscopy (Zeiss Observer Z1). Besides, fixed cells were dehydrated in graded ethanol series (50%, 70%, 80%, 90% and 100%) then cell attachment and cell spreading on scaffolds were observed with SEM analysis.

2.4.3. Cytotoxicity determination

Cytotoxicity of CH/FS composite scaffolds on SaOS-2 cell line were evaluated using indirect extraction method by WST-1 colorimetric assay according to ISO-10993 standard. Optical density was obtained at 440 nm wavelength by normalizing to cell viability. Results were calculated by using following equation:

$$\text{Cell viability\%} = \frac{\text{Average absorbance value of treated samples}}{\text{Average absorbance value of control}} \times 100 \quad (4)$$

2.4.4. Alkaline phosphatase (ALP) activity

ALP activity of SaOS-2 cells on the CH/FS composite scaffolds was quantified with osteogenic medium ($1\text{ }\mu\text{L/mL}$ L-ascorbic acid, $10\text{ }\mu\text{L/mL}$ β -glycerophosphate in complete medium) on 7, 14 and 21 days. Intracellular ALP activity was measured by fluorometric StemTAG™ ALP activity kit and extracellular ALP activity was measured with colorimetric kit Enzyline PAL Optimise kit according to the manufacturer's protocols.

2.4.5. Osteocalcin secretion

SaOS-2 cells were cultured on CH/FS composite scaffolds up to 28 days of incubation time in osteogenic medium as individual experiment sets. Osteocalcin (OC) secretion of SaOS-2 cells cultured on scaffolds was determined using Osteocalcin ELISA Kit. Culture media extracted from scaffolds were analyzed for determination of the OC concentrations on 21 and 28 days of culture.

2.4.6. Biomineralization

Alizarin Red and von Kossa staining are commonly used for detection calcium and phosphatase within the mineral deposition [27,28]. Alizarin Red S and von Kossa staining were performed to detect phosphate and calcium mineral deposition of cells on composite scaffolds. Firstly, fixation process was carried out with 3.7% paraformaldehyde for 20 min at room temperature. Scaffolds were washed with distilled water and cells were incubated with the corresponding staining solutions: for von Kossa staining, scaffolds were incubated with 1% (w/v) silver nitrate solution for 30 min under UV light. After three additional washing steps, scaffolds incubated with 5% (w/v) sodium thiosulfate solution for 5 min to remove unreacted silver. For Alizarin Red staining scaffolds were stained with 2% (w/v) Alizarin Red solution (pH 4.0) and incubated at room temperature in the dark for 30 min. Stained scaffolds were washed with distilled water several times to remove stain residue. Calcium and phosphatase mineral depositions were evaluated by stereomicroscope (Olympus, SOIF DA 0737). Besides, Alizarin Red S extracts were analyzed with semi-quantitatively at 405 nm to determine the differences of calcium mineral deposition.

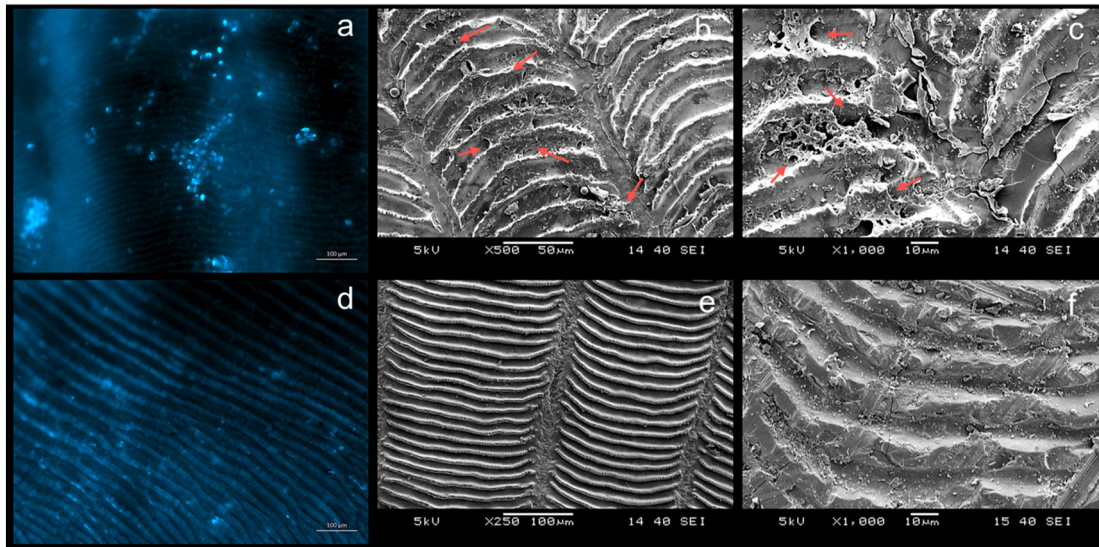


Fig. 1. SEM and fluorescence images of before (a, b, c) and after (d, e, f) decellularization process of the FS. Red arrows indicate that colonized FS cells.

2.5. Statistical analysis

The experimental data is presented as mean \pm standard deviation (SD). The differences between groups were analyzed using two-way Analysis of Variance (ANOVA) with Tukey's multiple comparison test. Mechanical test data were obtained by One-way ANOVA with Tukey's multiple comparison test. All p-values less than 0.05 were considered to be significant.

3. Results and discussion

3.1. Verification of decellularization process

SEM analysis and fluorescence microscopy images indicated that FS were successfully decellularized chemically (Fig. 1). Cells localized between microchannel were removed from the FS structure after decellularization. Fluorescence images showed that round shape cells were distributed homogenously on the untreated FS (Fig. 1a) and no cell nuclei on decellularized FS were found after

decellularization process as expected (Fig. 1d). SEM images also showed that FS possessed highly organized microstructure with cells between microchannel (Fig. 1b, c). Similar to the fluorescence results, cells were removed successfully, and the fibrillary collagen structure was not affected after the decellularization process (Fig. 1e, f). In addition to SEM and fluorescence analyses, histological staining was used to examine the decellularization process on FS (Fig. 2). Cells on FS were stained with Hematoxylin & eosin (HE) whereas, collagen structure was shown with Masson trichrome staining. In addition, type I and type II collagen in the structure were stained immunohistochemically. Histology results showed that cellular components of the FS were removed successfully without any deformation in chemical decellularization process. Distinctive arranged collagen fibers in FS stained with Masson trichrome staining and represented as blue in the structure. Histology results showed that collagen fibers were not influenced after decellularization. Type I collagen is one of the main components in FS structure was observed as dark brown. Immunohistochemical staining indicated that collagen type I was present in FS structure

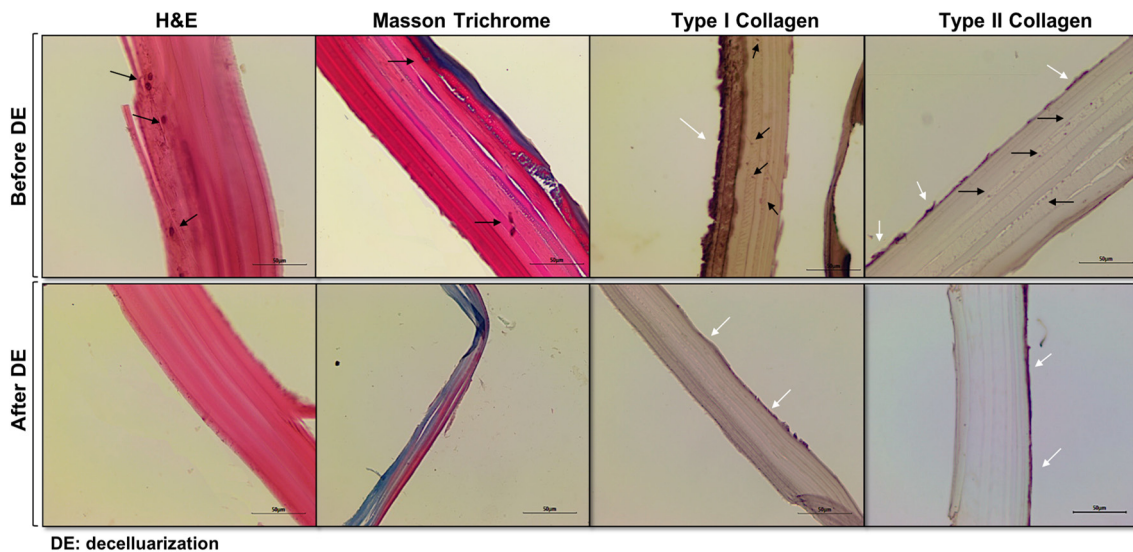


Fig. 2. Histological staining of the FS after and before decellularization. Black arrows indicate that FS cells, white arrows indicate that collagen structures in the FS.

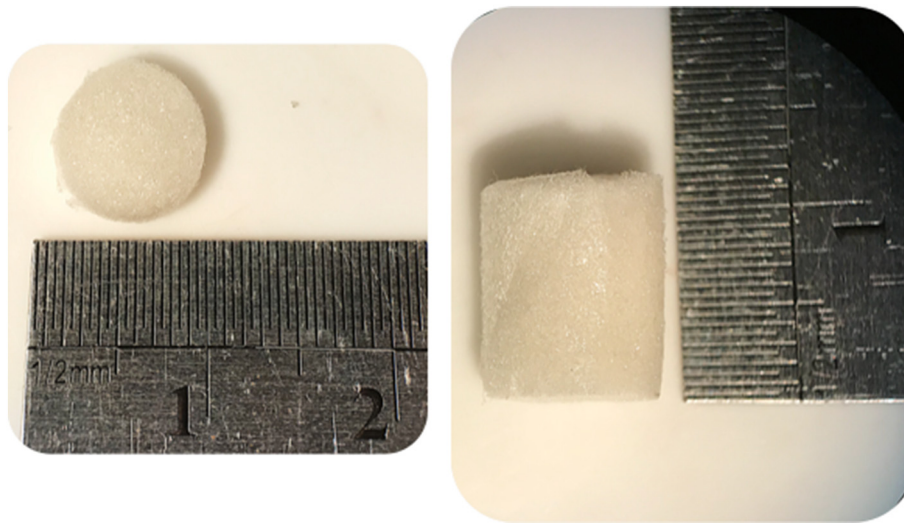


Fig. 3. Stereomicroscopy images of CH/FS composite scaffold.

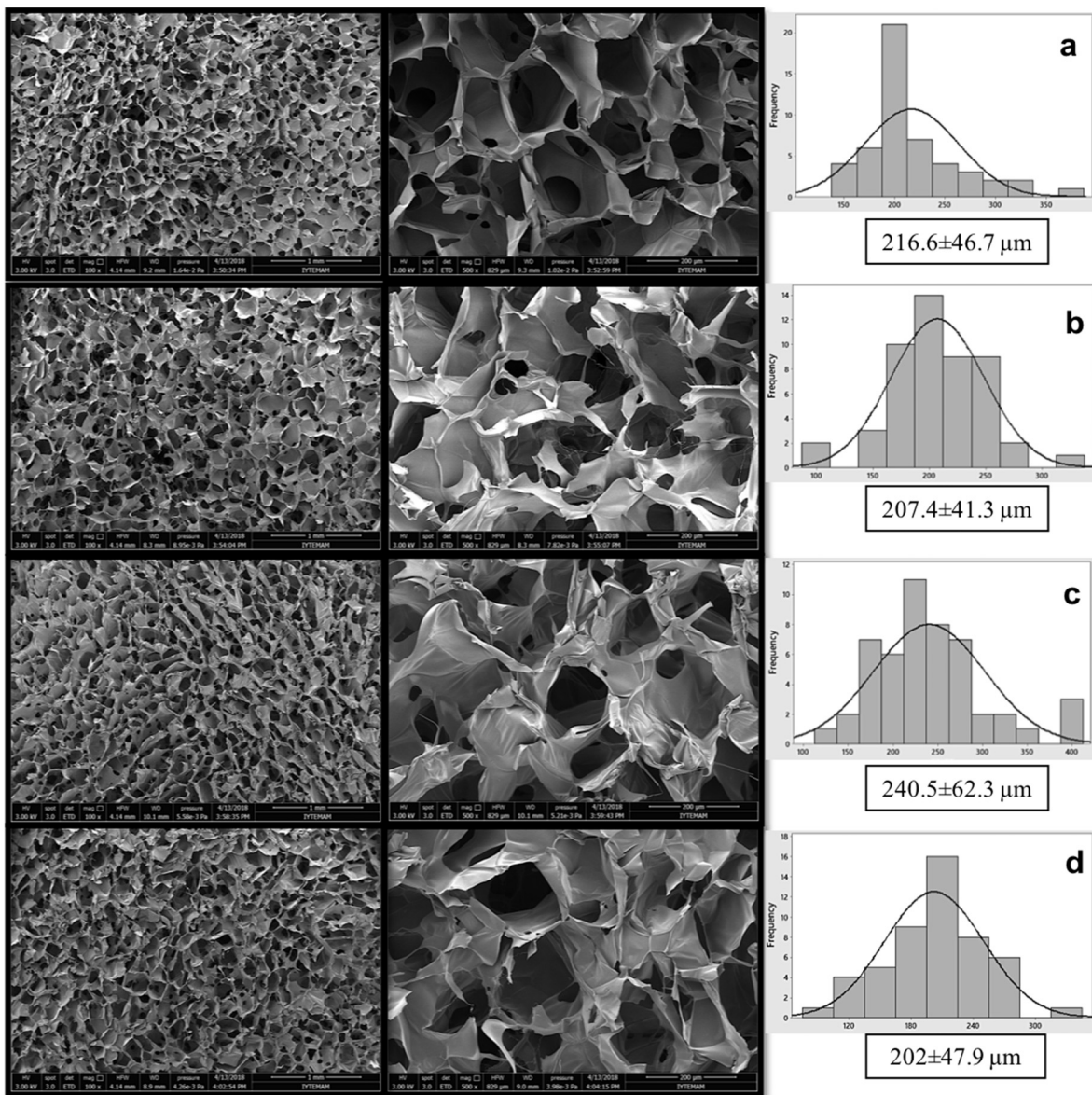


Fig. 4. SEM micrograph and pore size distribution of CH/FS composite scaffolds. a. CH, b. CH/3%FS, c. CH/6%FS, d. CH/10%FS.

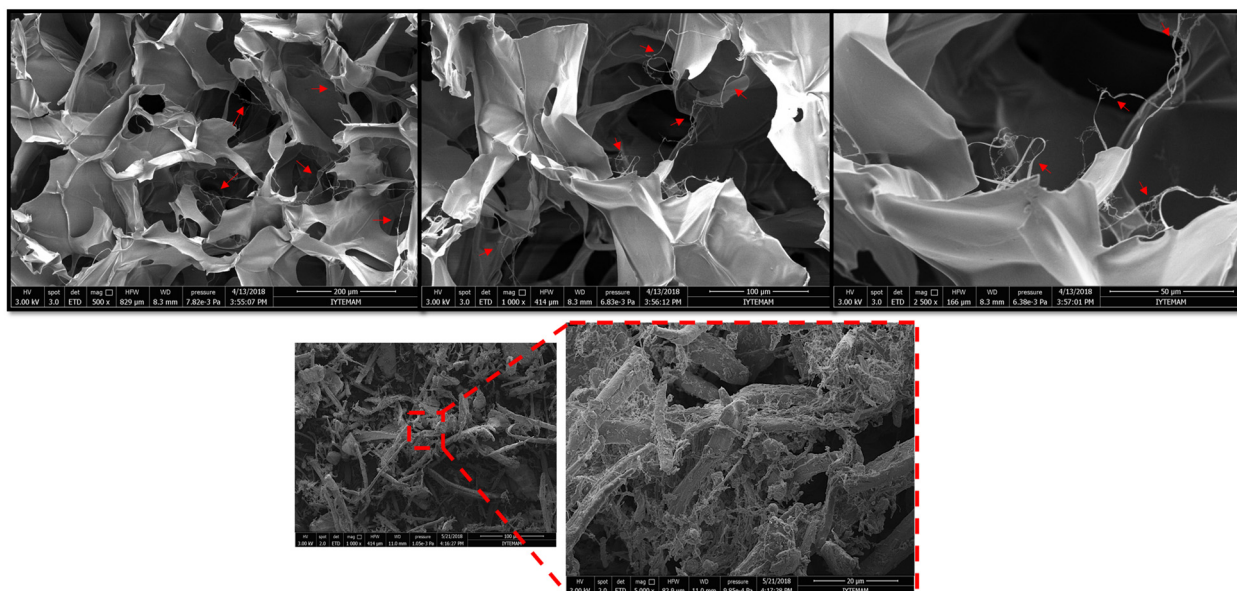


Fig. 5. SEM images of fibrillary FS structures (red arrows) in CH matrix.

after decellularization process as expected. It was observed as dark brown in FS structure. On the other hand, collagen type II which has weak immunopositivity in FS, was observed as light brown. Consequently, both type I and type II collagen were detected in FS structure immunohistochemically.

3.2. Characterization of the composite scaffolds

3.2.1. Morphology and porosity of CH/FS composite scaffolds

Stereomicroscopy images showed that CH/FS scaffolds were fabricated successfully by freeze drying method and possessed homogeneous structure and morphology with distinct dimensions (Fig. 3). The microstructure, morphology and pore size distribution of CH/FS composite scaffolds were investigated with SEM analysis (Figs. 4 and 5). Highly porous uniform structures were obtained with freeze-drying method. Minimum pore size of 100 μm is required critical for the diffusion of nutrients and oxygen for cell survival [1]. Average pore size range was obtained as 202–240 μm which is found to be appropriate for bone cell proliferation, tissue ingrowth, nutrient delivery and bone tissue vascularization [29,30] (Fig. 4). FS incorporation did not significantly affect the average pore size range of scaffolds compare to neat CH matrix. However, pore wall surface enlarged, and walls tightened on composite scaffolds. FS microparticles were also observed with their fibrillary structures embedded in CH matrix (Fig. 5). Lin et al. also observed the microchannels of FS that are composed of fibrillary structure [13].

3.2.2. Porosity and water uptake capacity of scaffolds

Cell migration is determined by degree of porosity and pore interconnectivity/tortuosity of scaffold. High porosity provides appropriate

micro-environment for nutrient delivery and vascularization for cell proliferation and differentiation at the defect site. In addition, scaffold architecture should mimic the structure of the targeted tissue. Trabecular bone has interconnected porous structure with a porosity range between 50 and 90% [31]. Thus, fabricated CH/FS composite scaffolds show appropriate structure for bone regeneration with high porosity changing in the range of 70–78% (Table 1).

Water uptake capacity of CH/FS scaffolds was determined to observe the possible swelling capacity of scaffolds at the defect site after implantation. Swelling property is an important factor for the interaction of the biomaterial and body fluids at the surrounding tissue. Scaffolds must absorb the body fluid to provide a physical and chemical interaction for protein adsorption which is the major factor for cell adhesion and response on material surface [32]. Swelling ratio % of scaffolds was obtained in a range of 270–342. Results showed that CS/FS scaffolds

Table 1

Porosity and water uptake capacity of the CH/FS composite scaffolds.

Groups	Porosity (%)	Water uptake capacity (24 h)
CH	69.8 \pm 1.58	270 \pm 4.27
CH/3%FS	73.4 \pm 6.76	309 \pm 8.29
CH/6%FS	84.5 \pm 9.69	306 \pm 4.14
CH/10%FS	77.7 \pm 11.12	342 \pm 3.12

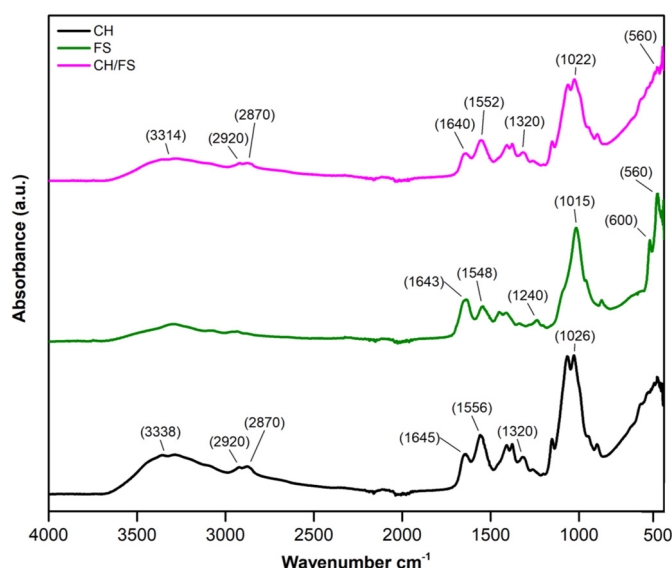


Fig. 6. FTIR-ATR spectrum of CH, FS and CH/10% FS composite scaffold.

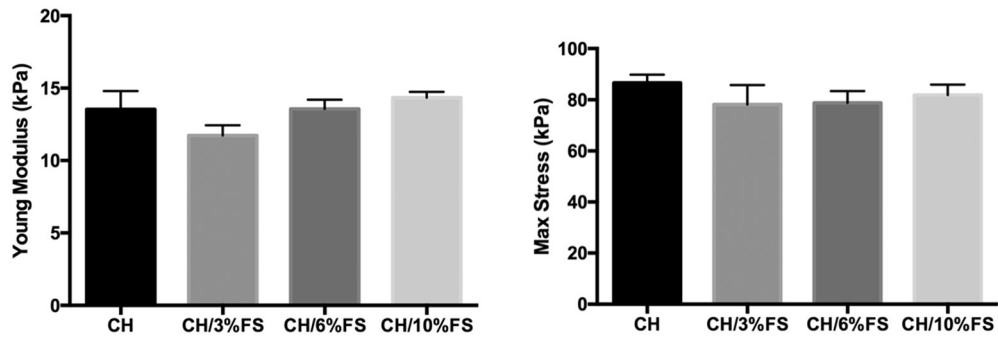


Fig. 7. Young Modulus and maximum stress of the CH and CH/FS composite scaffolds.

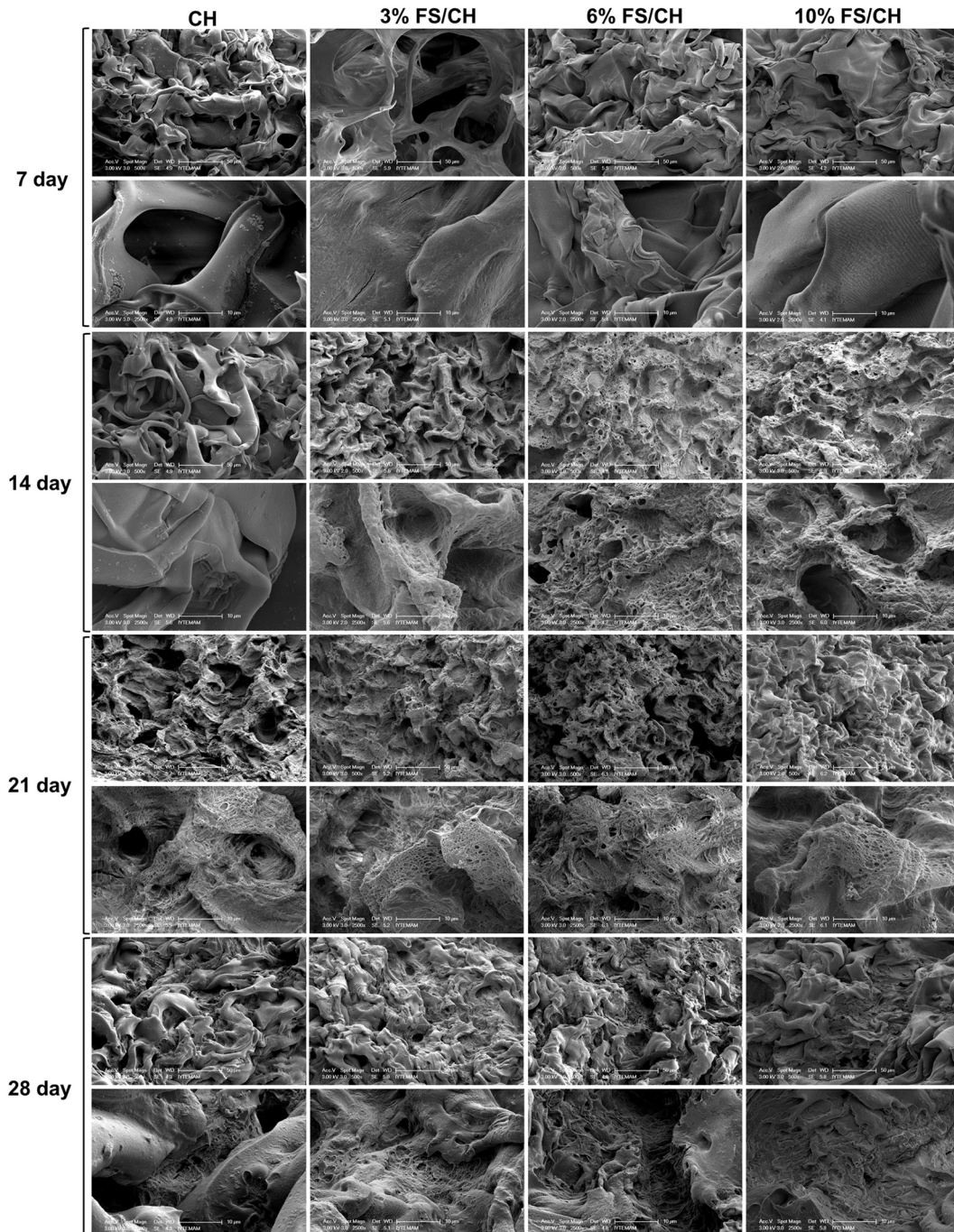


Fig. 8. SEM images of scaffolds after degradation process.

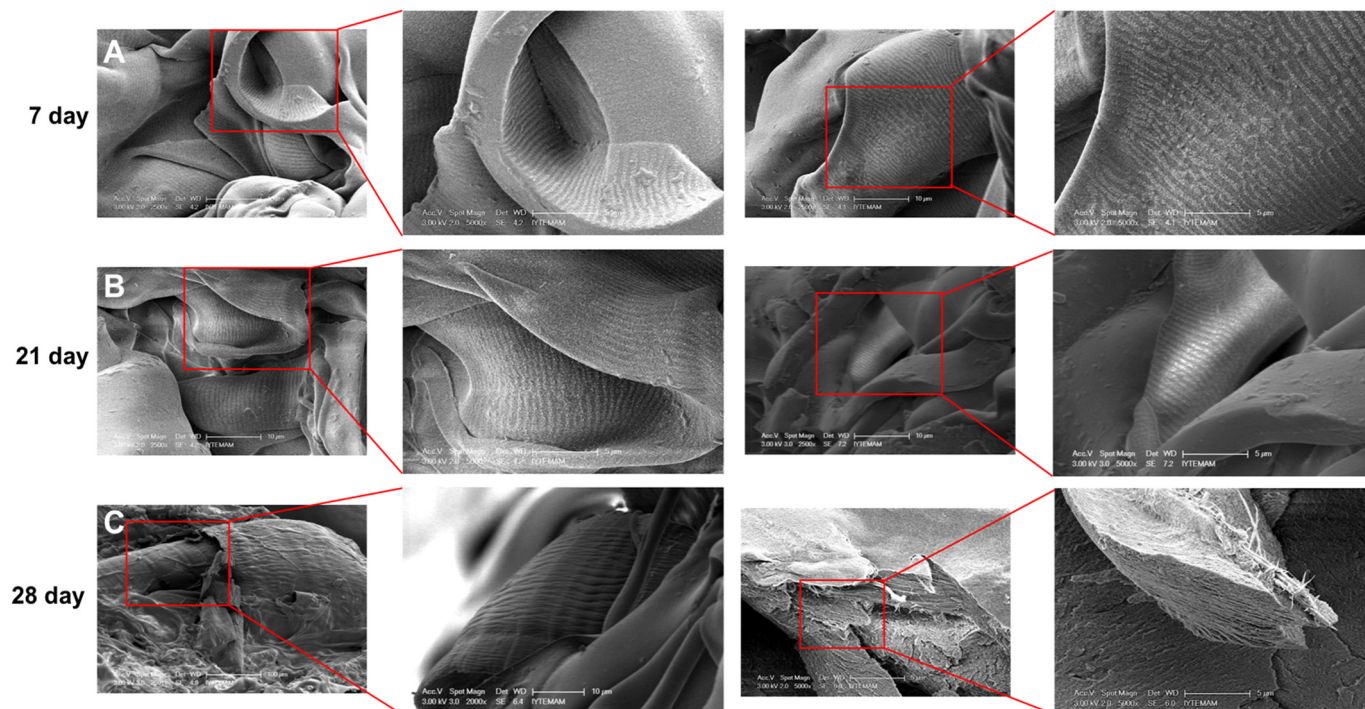


Fig. 9. SEM images of fish scales in composite scaffolds after degradation process.

highly absorbed the PBS in 24 h. FS particles enhanced the water uptake capacity of CS matrix.

3.2.3. FTIR analysis

FTIR analysis was performed to observe the integration of FS particles with chitosan matrix. In addition, the effect of degradation process on chemical structure of the composite scaffolds was investigated. Fig. 6 shows the FTIR spectra of the FS particles, CH and CH/FS composite scaffolds. FTIR spectrum of fish scales exhibited main characteristic absorption bands of collagen, ascribed to amide I, II and III of type I collagen which were observed at 1643 cm^{-1} , 1548 cm^{-1} and 1240 cm^{-1} respectively. In addition, P—O stretching band at around 1015 cm^{-1} and P—O bending bands at 600 and 560 cm^{-1} are assigned to the O—P—O bending mode of the Hap [33]. Basic characteristic peaks of chitosan were shown as C—H stretching at 2870 and CH_2 vibrations at 2920 cm^{-1} , stretching vibrations of O—H groups at 3338 cm^{-1} . Besides, the bands at 1645 cm^{-1} , 1556 cm^{-1} and 1320 cm^{-1} were attributed to Amide I, —NH₂ bending and Amide III, respectively [34,35]. In the spectra of CH/FS composite scaffolds, both characteristic peaks of chitosan and fish scale are exhibited which proved that fish scales were successfully incorporated into the chitosan matrix.

3.2.4. Mechanical properties

Mechanical properties of CH/FS composite scaffolds were evaluated by compression test. Compressive modulus of the scaffolds were calculated from the initial linear part of the stress-strain curves. Composite scaffolds exhibited similar compression modulus and max. stress with CH scaffolds in a range of $13.5\text{--}14.3\text{ kPa}$. Increasing FS microparticle reinforcement content quietly increased the Young modulus positively (Fig. 7). However, there are no statistically significant differences between groups.

3.2.5. Degradation rate of composite scaffolds

Degradation of polymeric biomaterials occurs by enzymatically either by oxidation or hydrolysis when they are in contact with the body fluids [36]. Therefore, degradation profile of CH/FS composite

scaffolds was investigated enzymatically in the presence of lysozyme which is one of the enzymes present in the human serum that can hydrolyze the $\beta(1\text{--}4)$ linkages between *N*-acetylglucosamine and glucosamine units in CH [37]. Degradation study was performed to observe the weight loss of the scaffolds which were incubated in enzymatic medium. The enzymatic degradation rate proceeds from the surface of the polymer. Thus, surface area and porosity of the scaffold control the degradation rate [38]. Therefore, morphological changes in the structure of the degraded scaffolds were observed with SEM analysis. Images showed that scaffold surface structure did not alter at early incubation periods (7th day). At 14th day of incubation, FS incorporation induced the disintegration of the pore walls of CH/FS scaffolds and pore wall surfaces started to exhibit porous structure (Fig. 8). However, FS particles remained embedded in chitosan matrix during degradation process and multipattern morphology of FS were observed on pore wall surfaces (Fig. 9). The degradation process of CH is generally dependent on the degree of acetylation which leads to faster degradation rate [39]. As a hydrophilic polymer, degradation of CH is formed via bulk erosion. Diffusion of water into CH matrices is faster than degradation. Thus, CH begins to swell and then degradation starts. In literature degradation of CH is defined as a process comprised of two main stages: interaction with water in the lysozyme solution causing hydration and swelling; bond cleavage causing degradation and weight loss [40]. All groups showed linear weight loss trend during 28 days of incubation. Results showed that, weight loss% for CH scaffolds was found as 46% whereas, 3%FS and 6%FS incorporation increased the weight loss from 46 to 50 and 66% at the end of 28 days, respectively. Maximum weight loss was observed for CS/6%FS composites (Fig. 10). This result is expected since CS/6%FS scaffolds possess higher pore size and porosity compared to 3% and 10% FS groups. Besides, it has been reported that FS are biodegraded in a short time in vivo [25]. Fig. 10 also shows the FTIR spectra both before and after the degradation of the CH/FS composite scaffolds. After degradation process, the amide III peak intensities of both chitosan and FS microparticles were found to be lower than in the composite structures before degradation.

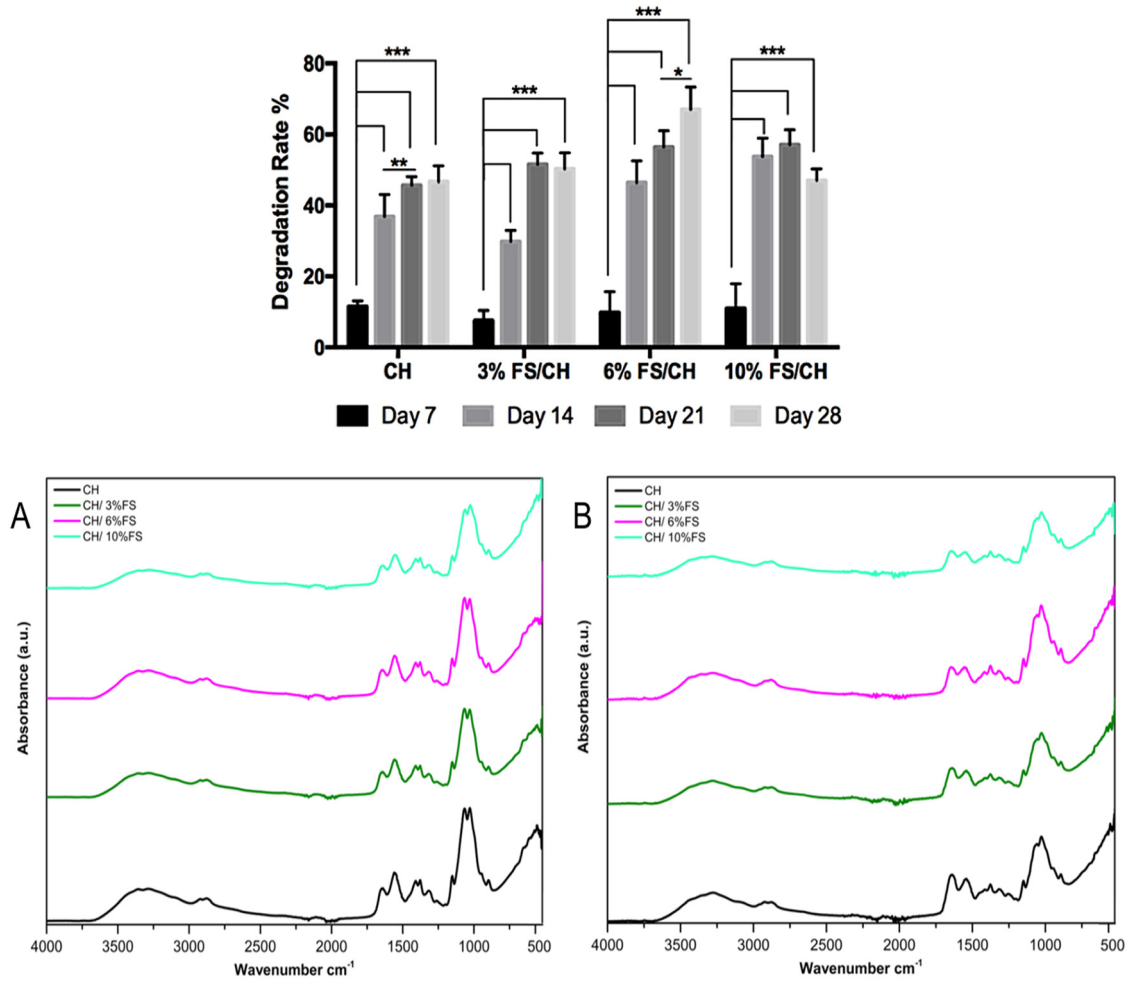


Fig. 10. Degradation rate of the scaffolds and FTIR-ATR spectrum of the CH and CH/FS composite scaffolds before (A) and after (B) degradation.

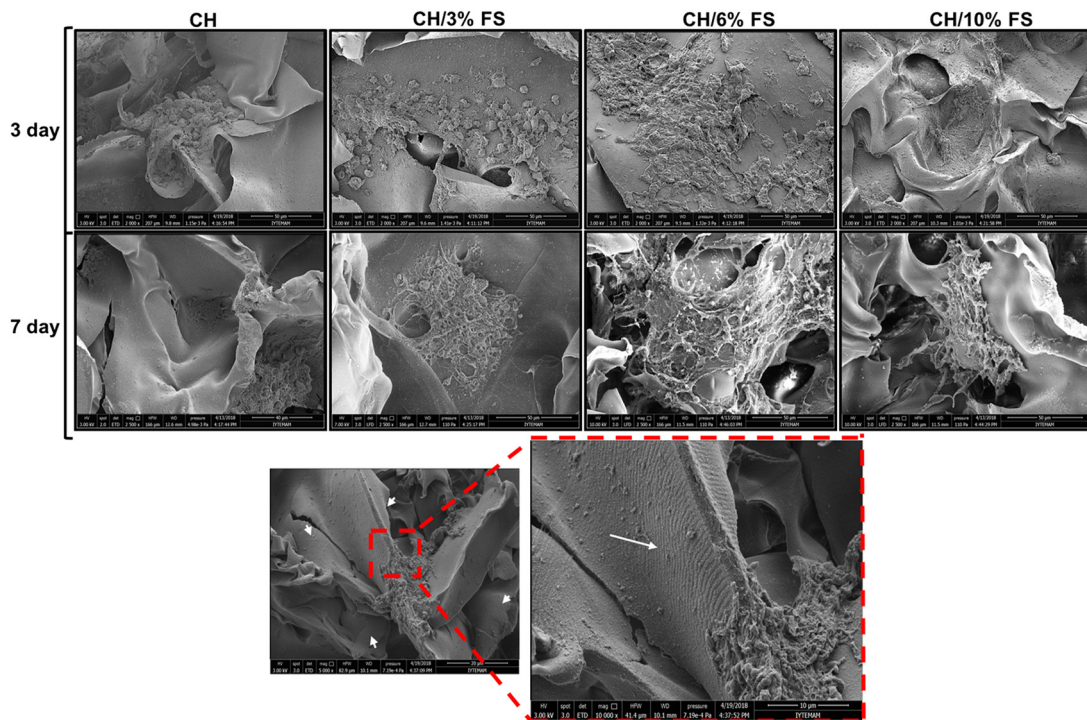


Fig. 11. SEM images showing SaOS-2 cell attachment and spreading on which show the FS microparticles embedded pore wall surface of CH/FS scaffolds.

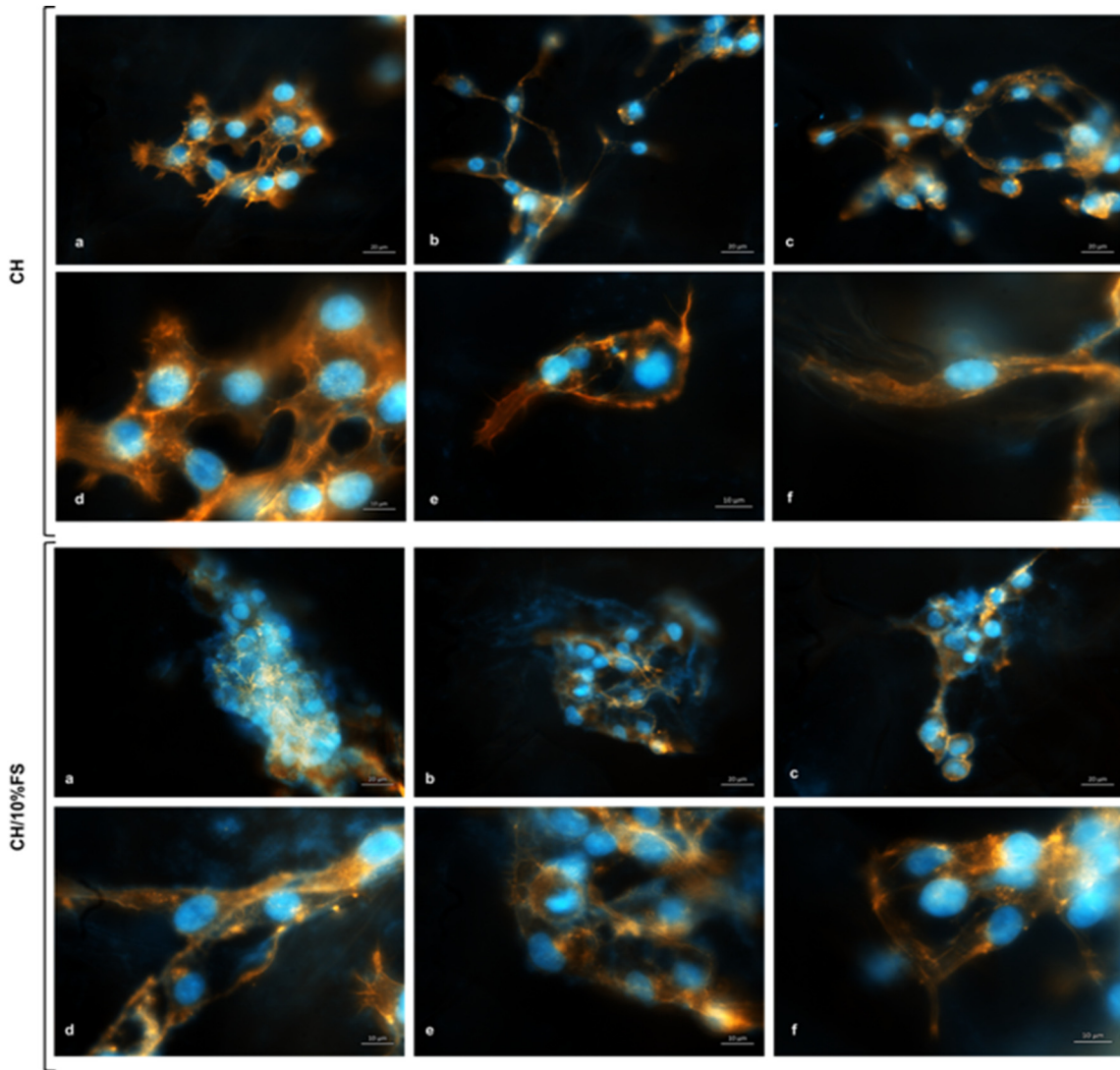


Fig. 12. SaOS-2 attachment on CH and CH/FS composite scaffolds for 14 days of incubation.

3.3. In vitro studies

3.3.1. Cell attachment and morphology

SaOS-2 cells incubated on CH/FS composite scaffolds were observed with SEM and fluorescence microscopy. Fluorescence and SEM images showed that SaOS-2 osteoblast like cells attached on pore wall surface

of scaffolds with their filapodial extensions and exhibited a lamellipodium formation on material surface (Figs. 11–12). FS incorporation altered the pore wall morphology by changing surface structure and increasing roughness. FS microparticles provided high surface area with microchannels and enhanced the cell attachment on scaffold surface. Lin and coworkers also investigated the effect of microchannel morphology on decellularized FS surface and stated that orientation of microchannels enhanced the cell attachment and guided cell proliferation [13]. This structure is shown in SEM images of cell attachment (Fig. 11). Thus, SaOS-2 cells on CH/FS scaffolds colonized on pore walls with clusters and showed more bone cell-like morphology compared to control group (Fig. 12).

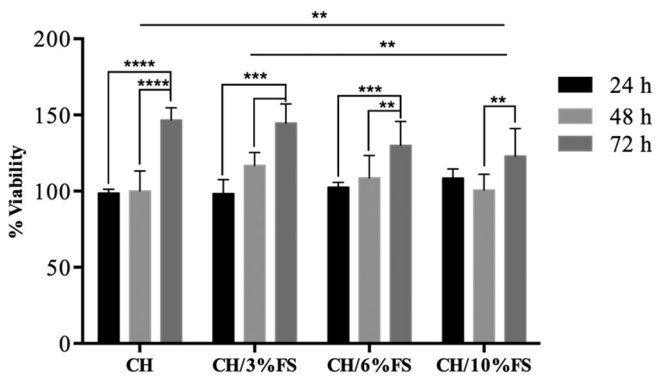


Fig. 13. Cell viability of SaOS-2 cells with scaffold extract.

3.3.2. Cytotoxicity

In vitro cytotoxicity of the scaffolds was evaluated by WST-1 assay with SaOS-2 cell line as specified in ISO standards (Fig. 13). Cell viability results represented that CH/FS scaffolds did not show any cytotoxic effect on SaOS-2 cell lines. Besides, cell viability has been shown to be sustained. At 3 and 6% FS incorporation, composite groups showed an increasing trend with incubation time and high cell viability was observed similar to pure CH group. Cell viability of SaOS-2 cells incubated with CH/10%FS extract decreased for 48 h incubation. However, it was found that the cell viability increased

at the end of 72 h incubation period. For all groups SaOS-2 viability increased by incubation period and these increases were found to be statistically significant.

3.3.3. Cell proliferation

SaOS-2 osteoblastic cell proliferation on CH/FS scaffolds were evaluated by WST-1 assay. It was found that SaOS-2 cells were proliferated on the composite scaffolds with an increasing trend between days 7, 10, 14 and 21 (Fig. 14). The absorbance values showed similar % cell viability for both CH and CH/FS composite scaffolds within the culture period. However, FS microparticle incorporation into CH matrix increased cell proliferation after 14th day of incubation. This inducing effect on bioactivity of composite scaffolds results from collagen and HAp content of FS. Absorbance differences were statistically significant between CH and CH/6–10% FS groups for 14 and 21 days of incubation.

3.3.4. Alkaline phosphatase (ALP) activity

ALP activity is known as an important osteogenic differentiation marker at the early stages of bone tissue regeneration. In literature, SaOS-2 is indicated as model cell line which possess higher ALP activity and matrix mineralization capacity with a more mature osteoblast phenotype [41]. It is also known that SaOS-2 cells show similar ALP activity and growth factor expression to human primary osteoblast cells at the early stage of differentiation [42–45]. Therefore, in this study Saos-2 cell line was used to investigate the effect of FS microparticles on ALP activity. Results indicated that FS microparticles induced both intracellular and extracellular ALP activity of Saos-2 cells incubated on CH scaffolds (Fig. 14). This enhancement arises from the collagen type I content of

FS microparticles. Since, as an important extracellular matrix component collagen induces osteoblastic differentiation. Besides, FS incorporation extended the ALP activity secretion to 21th day of incubation. Increasing FS content significantly affected the ALP activity of Saos-2 cells showing an increasing trend with incubation time. At 21th day of incubation, 10% FS incorporation significantly enhanced the extracellular ALP activity compared to pure CH scaffold. In addition, statistically significant differences were obtained between FS incorporated groups and CH scaffolds at 7,14 and 21 days of incubation. Therefore, in this study Saos-2 cell line was used to investigate the effect of FS microparticles on ALP activity.

3.3.5. Osteocalcin secretion

Osteocalcin (OC) which is a bone-specific protein synthesized by osteoblasts is known as an important marker for osteogenic maturation by coordinating organic matrix and bone mineral formation. Osteocalcin is generally used as a serum marker and it is known to act as a regulator for bone matrix mineralization [46,47]. In this study, osteocalcin (OC) secretion of SaOS-2 cells on scaffolds was investigated for 21 and 28 days of incubation. ELISA results indicated that 3–6% FS incorporation enhanced the OC secretion significantly at 28th day of incubation. In addition, OC secretion showed an increasing trend with incubation time on CH/FS composite scaffolds. However, OC secretion decreased with incubation time on CH scaffolds (Fig. 14).

3.3.6. Biomineralization

Ca and P deposition on scaffolds was detected with Alizarin Red S and von Kossa staining respectively. Scaffolds stained and observed

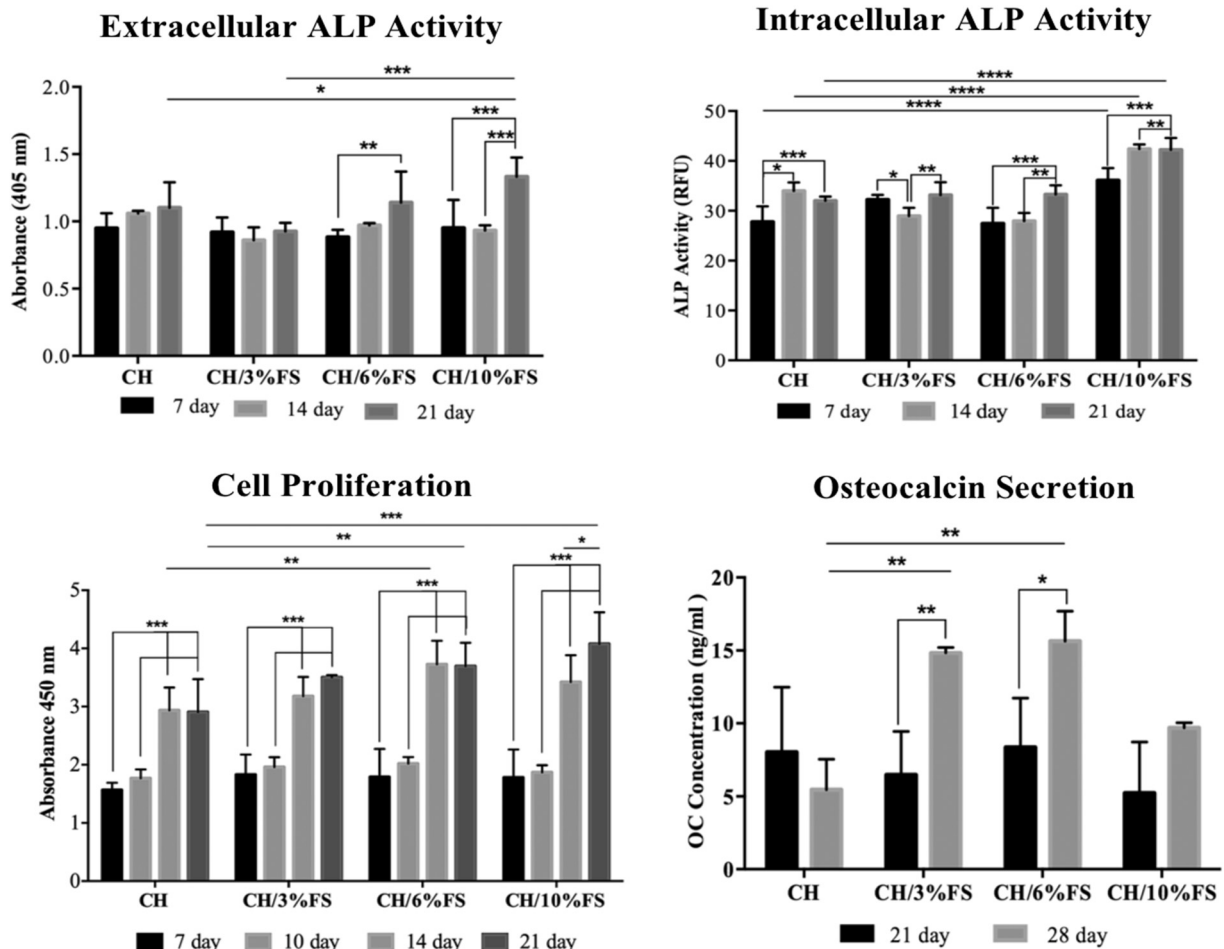


Fig. 14. ALP activity, proliferation and OC secretion of the SaOS-2 cells on the scaffolds.

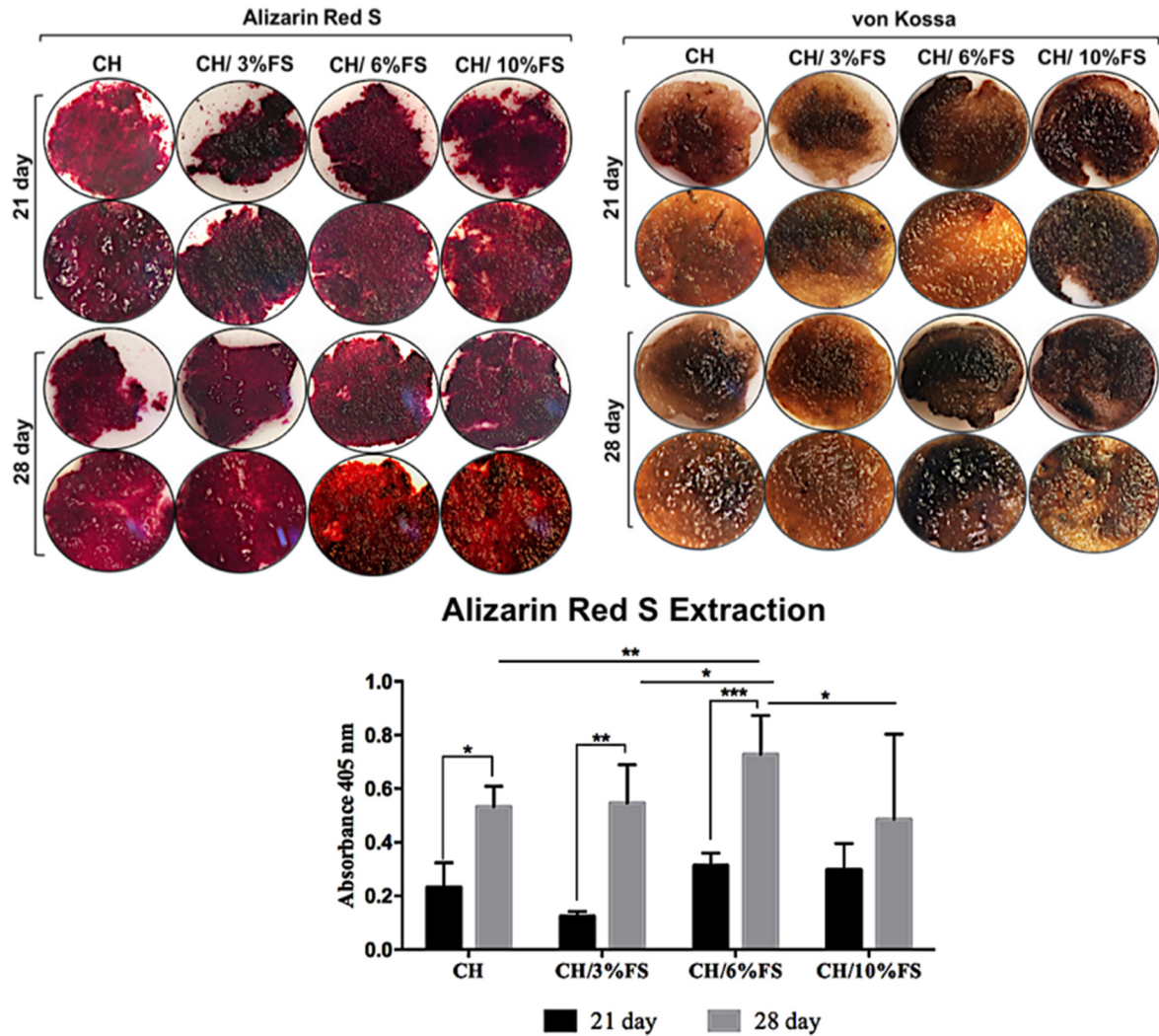


Fig. 15. Alizarin Red S and Von Kossa staining of the biomaterialized scaffold and Alizarin Red S extraction of the SaOS-2 cells on the composite scaffolds.

with stereomicroscopy to investigate the biomineralization on surface (Fig. 15). In addition, biomineralization on surface was observed with SEM analysis using backscatter mode (Fig. 16). Stereoimages showed that all groups induced biomineralization with Ca and P deposition. At 28th day, both Alizarin Red S and von Kossa stained CH/FS composite scaffolds showed darker red and brownish colour on the surface. This colour change results from higher Ca/P deposition. However, differences between groups could not be detected quantitatively from images. Thus, Alizarin Red S extraction method was used to detect biomineralization quantitatively. Ca deposition was significantly enhanced by FS incorporation at 28th day of incubation (Fig. 15). Von Kossa images showed that 6–10% FS incorporation significantly increased P deposition on scaffold surface for 21 and 28 days of incubation. Results indicated that HAp content of FS microparticles significantly induced biomineralization on CH matrix. SEM images also demonstrated the enhanced biomineralization around SaOS-2 cells on composite scaffold surface for 14 and 28 days of incubation compared to net CH surface (Fig. 16).

4. Conclusion

In this study, novel CH/FS composite scaffolds were fabricated for bone tissue regeneration. FS were successfully decellularized and physically fragmented into microparticles to incorporate into CH matrix. Results showed that CH/FS composites were obtained as highly porous

scaffolds in which FS microparticles were embedded as fibrillary structures and multipattern morphology of FS were observed on pore wall surface of chitosan matrix. Scaffold surface structure did not alter at early incubation periods of degradation. After 14 days of incubation, FS incorporation enhanced degradation rate in CH matrix by inducing the disintegration of the pore wall structures and high porosity on pore surfaces. However, no significant change was observed in mechanical properties by FS incorporation. Microchannel morphology of FS altered the surface roughness and pore wall structures of CH scaffolds which affected cell attachment positively. FS incorporation also increased the cytocompatibility and proliferation of SaOS-2 cells on CH scaffolds with its collagen content. FS incorporated scaffolds induced ALP activity, osteocalcin secretion and biomineralization which are major osteogenic markers osteoblast differentiation and bone regeneration. This inducing effect resulted from composition of FS microparticles with regard to its high collagen and Hap content. Consequently, FS microparticles which have structural similarity with bone can be considered as a potential bioactive reinforcement in polymeric scaffolds for bone tissue engineering applications.

Acknowledgments

The authors thank Assistant Professor Dr. Meltem Alper from Aksaray University for supplying SaOS-2 cell line. The authors are grateful to Izmir Institute of Technology Biotechnology and Bioengineering

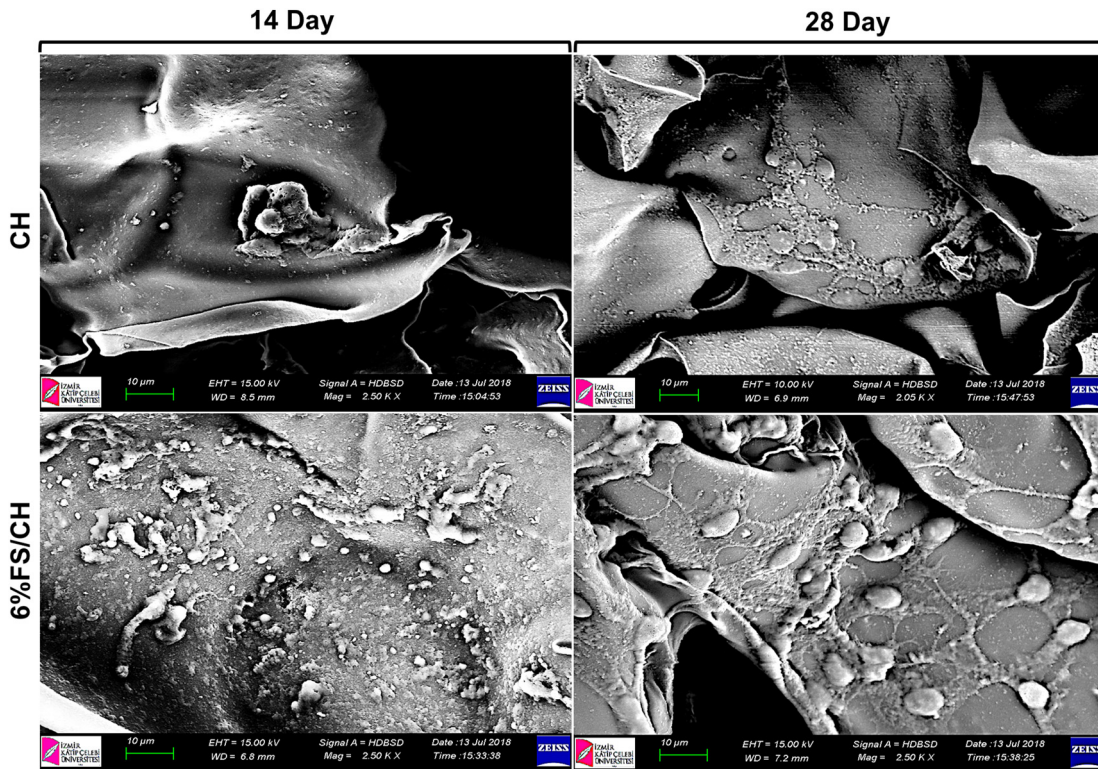


Fig. 16. SEM images of the biom mineralized matrix on the scaffolds.

Research and Application Center (IYTE BIOMER) and Center for Materials Research (IZTECH MAM) for fluorescence microscopy and SEM analyses. This research did not receive any specific grant from funding agencies in the public, commercial, or not-for-profit sectors.

References

- [1] S. Bose, M. Roy, A. Bandyopadhyay, Recent advances in bone tissue engineering scaffolds, *Trends Biotechnol.* 30 (10) (2012) 546–554.
- [2] A.R. Amini, C.T. Laurencin, S.P. Nukavarapu, Bone tissue engineering: recent advances and challenges, *Crit. Rev. Biomed. Eng.* 40 (5) (2012) 363–408.
- [3] M.M. Stevens, Biomaterials for bone tissue engineering, *Mater. Today* 11 (5) (2008) 18–25.
- [4] G. Turnbull, et al., 3D bioactive composite scaffolds for bone tissue engineering, *Bioact. Mater.* 3 (3) (2017) 278–314.
- [5] P.X. Ma, J.W. Choi, Biodegradable polymer scaffolds with well-defined interconnected spherical pore network, *Tissue Eng.* 7 (1) (2001) 23–33.
- [6] M.A. Woodruff, D.W. Hutmacher, The return of a forgotten polymer - polycaprolactone in the 21st century, *Prog. Polym. Sci.* 35 (10) (2010) 1217–1256.
- [7] S.J. Hollister, W.L. Murphy, Scaffold translation: barriers between concept and clinic, *Tissue Eng. Part B Rev.* 17 (6) (2011) 459–474.
- [8] S. Stratton, N.B. Shelke, K. Hoshino, S. Rudraiah, S.G. Kumbar, Bioactive polymeric scaffolds for tissue engineering, *Bioact. Mater.* 1 (6) (2016) 93–108.
- [9] H.Ç. Arca, S. Şenel, "Chitosan based systems for tissue engineering part 1: hard tissues," *FABAD, J. Pharm. Sci.* vol. 33, no. 2008 (March 2008) 35–49.
- [10] I.-Y. Kim, et al., Chitosan and its derivatives for tissue engineering applications, *Biotechnol. Adv.* 26 (1) (2008) 1–21.
- [11] T. Ikoma, H. Kobayashi, J. Tanaka, D. Walsh, S. Mann, Microstructure, mechanical, and biomimetic properties of fish scales from *Pagrus major*, *J. Struct. Biol.* 142 (3) (2003) 327–333.
- [12] J.R. Metz, E. de Vrieze, E.J. Lock, I.E. Schulten, G. Flik, Elasmoid scales of fishes as model in biomedical bone research, *J. Appl. Ichthyol.* 28 (3) (2012) 382–387.
- [13] C.C. Lin, et al., A new fish scale-derived scaffold for corneal regeneration, *Eur. Cells Mater.* 26 (19) (2010) 50–57.
- [14] M. Okuda, et al., Minerals and aligned collagen fibrils in tilapia fish scales: structural analysis using dark-field and energy-filtered transmission electron microscopy and electron tomography, *Microsc. Microanal.* 15 (05) (2011) 788–798.
- [15] P. Jana, T. Mitra, T.K.R. Selvaraj, A. Gnanamani, P.P. Kundu, Preparation of guar gum scaffold film grafted with ethylenediamine and fish scale collagen, cross-linked with ceftazidime for wound healing application, *Carbohydr. Polym.* 153 (2016) 573–581.
- [16] T.H. van Essen, et al., Biocompatibility of a fish scale-derived artificial cornea: cytotoxicity, cellular adhesion and phenotype, and in vivo immunogenicity, *Biomaterials* 81 (2016) 36–45.
- [17] B. Kaczmarek, A. Sionkowska, A.M. Osyczka, Collagen-based scaffolds enriched with glycosaminoglycans isolated from skin of *Salmo salar* fish, *Polym. Test.* 62 (2017) 132–136.
- [18] Q. Li, et al., A novel fish collagen scaffold as dural substitute, *Mater. Sci. Eng. C* 80 (2017) 346–351.
- [19] B. Mondal, S. Mondal, A. Mondal, N. Mandal, Fish scale derived hydroxyapatite scaffold for bone tissue engineering, *Mater. Charact.* 121 (2016) 112–124.
- [20] S. Mondal, U. Pal, A. Dey, Natural origin hydroxyapatite scaffold as potential bone tissue engineering substitute, *Ceram. Int.* 42 (16) (2016) 18338–18346.
- [21] W. Pon-On, P. Suntornsaratoon, N. Charoenphandhu, J. Thongbunchoo, N. Krishnamra, I.M. Tang, Hydroxyapatite from fish scale for potential use as bone scaffold or regenerative material, *Mater. Sci. Eng. C* (2016).
- [22] D.J. Choi, et al., Bioactive fish collagen/polycaprolactone composite nanofibrous scaffolds fabricated by electrospinning for 3D cell culture, *J. Biotechnol.* 205 (2015) 47–58.
- [23] Z. Fang, Y. Wang, Q. Feng, A. Kienzle, W.E.G. Müller, Hierarchical structure and cytocompatibility of fish scales from *Carassius auratus*, *Mater. Sci. Eng. C* 43 (2014) 145–152.
- [24] K. Yamamoto, et al., Biological safety of fish (tilapia) collagen, *Biomed. Res. Int.*, 2014.
- [25] C.-H. Chou, Y.-G. Chen, C.-C. Lin, S.-M. Lin, K.-C. Yang, S.-H. Chang, Bioabsorbable fish scale for the internal fixation of fracture: a preliminary study, *Tissue Eng. Part A* 20 (17–18) (2014) 2493–2502.
- [26] S.F. Badylak, D.O. Freytes, T.W. Gilbert, Reprint of: extracellular matrix as a biological scaffold material: structure and function, *Acta Biomater.* 23 (2015) 17–26.
- [27] C.D. Hoemann, H. El-Gabalawy, M.D. McKee, In vitro osteogenesis assays: influence of the primary cell source on alkaline phosphatase activity and mineralization, *Pathol. Biol.* 57 (4) (2009) 318–323.
- [28] X. Zhang, et al., Polymer-ceramic spiral structured scaffolds for bone tissue engineering: effect of hydroxyapatite composition on human fetal osteoblasts, *PLoS One* 9 (1) (2014), e85871.
- [29] C.M. Murphy, M.G. Haugh, F.J. O'Brien, The effect of mean pore size on cell attachment, proliferation and migration in collagen-glycosaminoglycan scaffolds for bone tissue engineering, *Biomaterials* 31 (3) (2010) 461–466.
- [30] Q. Chen, J. Roether, A. Boccacini, Tissue engineering scaffolds from bioactive glass and composite materials, *Top. Tissue Eng.* 4 (6) (2008) 1–27.
- [31] A.R. Costa-Pinto, R.L. Reis, N.M. Neves, Scaffolds based bone tissue engineering: the role of chitosan, *Tissue Eng. Part B Rev.* 17 (5) (2011) 331–347.
- [32] R. Latour, Biomaterials: protein-surface interactions, *Encyclopedia of Biomaterials and Biomedical Engineering*, Second Edition-Four Volume Set, 2008.
- [33] W.T. Liu, Y. Zhang, G.Y. Li, Y.Q. Miao, X.H. Wu, Structure and composition of teleost scales from snakehead *Channa argus* (Cantor) (Perciformes: Channidae), *J. Fish Biol.* 72 (4) (2008) 1055–1067.
- [34] I. Corazzari, et al., Advanced physico-chemical characterization of chitosan by means of TGA coupled on-line with FTIR and GCMS: thermal degradation and water adsorption capacity, *Polym. Degrad. Stab.* 112 (2015) 1–9.

- [35] S. Tamburaci, F. Tihminlioglu, Diatomite reinforced chitosan composite membrane as potential scaffold for guided bone regeneration, *Mater. Sci. Eng. C* 80 (2017) 222–231.
- [36] H. Azevedo, R. Reis, Understanding the enzymatic degradation of biodegradable polymers and strategies to control their degradation rate, *Biodegradable Systems in Tissue Engineering and Regenerative Medicine*, 2004.
- [37] T. Freier, H.S. Koh, K. Kazazian, M.S. Shoichet, Controlling cell adhesion and degradation of chitosan films by N-acetylation, *Biomaterials* 26 (29) (2005) 5872–5878.
- [38] H.Y. Cheung, K.T. Lau, T.P. Lu, D. Hui, A critical review on polymer-based bio-engineered materials for scaffold development, *Compos. Part B Eng.* 383 (3) (2007) 291–300.
- [39] T. Kean, M. Thanou, Biodegradation, biodistribution and toxicity of chitosan, *Adv. Drug Deliv. Rev.* 62 (1) (2010) 3–11.
- [40] D. Ren, H. Yi, W. Wang, X. Ma, The enzymatic degradation and swelling properties of chitosan matrices with different degrees of N-acetylation, *Carbohydr. Res.* 340 (15) (2005) 2403–2410.
- [41] E. Murray, D. Provedini, D. Curran, B. Catherwood, H. Sussman, S. Manolagas, Characterization of a human osteoblastic osteosarcoma cell line (SAOS-2) with high bone alkaline phosphatase activity, *J. Bone Miner. Res.* 2 (3) (1987) 231–238.
- [42] L. Saldaña, F. Bensiamar, A. Boré, N. Vilaboa, In search of representative models of human bone-forming cells for cytocompatibility studies, *Acta Biomater.* 7 (12) (2011) 4210–4221.
- [43] G. Bilbe, E. Roberts, M. Birch, D.B. Evans, PCR phenotyping of cytokines, growth factors and their receptors and bone matrix proteins in human osteoblast-like cell lines, *Bone* 19 (5) (1996) 437–445.
- [44] L.G. Rao, M.K. Sutherland, G.S. Reddy, M.L. Siu-Caldera, M.R. Uskokovic, T.M. Murray, Effects of 1 α , 25-dihydroxy-16ene, 23yne-vitamin D3 on osteoblastic function in human osteosarcoma SaOS-2 cells: differentiation-stage dependence and modulation by 17-beta estradiol, *Bone* 19 (6) (1996) 621–627.
- [45] E.M. Czekanska, M.J. Stoddart, R.G. Richards, J.S. Hayes, In search of an osteoblast cell model for in vitro research, *Eur. Cell. Mater.* 24 (2012).
- [46] A. Nakamura, et al., Osteocalcin secretion as an early marker of in vitro osteogenic differentiation of rat mesenchymal stem cells, *Tissue Eng. Part C. Methods* 15 (2) (2009) 169–180.
- [47] M.L. Zoch, T.L. Clemens, R.C. Riddle, New insights into the biology of osteocalcin, *Bone* 82 (2016) 42–49.